An Organic Donor/Acceptor Lateral Superlattice at the Nanoscale

Roberto Otero,[†] David Écija,[†] Gustavo Fernández,[‡] José María Gallego,[§] Luis Sánchez,[‡] Nazario Martín,*[,‡,||] and Rodolfo Miranda*[,†,||]

Departamento de Física de la Materia Condensada, Universidad Autónoma de Madrid, 28049 Madrid, Spain, Departamento de Química Orgánica, Universidad Complutense de Madrid, 28040 Madrid, Spain, and Instituto de Ciencia de Materiales de Madrid−CSIC, 28049 Madrid, Spain

ABSTRACT

A precise control of the nanometer-scale morphology in systems containing mixtures of donor/acceptor molecules is a key factor to improve the efficiency of organic photovoltaic devices. Here we report on a scanning tunneling microscopy study of the first stages of growth of 2-[9-(1,3-dithiol-2-ylidene)anthracen-10(9H)-ylidene]-1,3-dithiole, as electron donor, and phenyl-C_{61}-butyric acid methyl ester, as electron acceptor, on a Au(111) substrate under ultrahigh vacuum conditions. Due to differences in bonding strength with the substrate and different interactions with the Au(111) herringbone surface reconstruction, mixed thin films spontaneously segregate into a lateral superlattice of interdigitated nanoscale stripes with a characteristic width of about 10−20 nm, a morphology that has been predicted to optimize the efficiency of organic solar cells.

Organic electron-donor/electron-acceptor blends are a key ingredient of "plastic" photovoltaic devices, whose development raises an ever-increasing scientific interest due to their low cost, easy production process, and mechanical flexibility.[1−4] The importance of blending donors and acceptors for the efficiency of solar cells rests on the capability of their interfaces to dissociate the tightly bound excitons that are generated in organic materials upon photon excitation, the formation and recombination of which is one of the major factors limiting the efficiency of photovoltaic devices.[1−4]

The role of donor/acceptor interfaces on the efficiency of photovoltaic devices implies that a number of criteria must be satisfied by the morphology of the blend for optimum solar cell performance: first, electron-donor and acceptor domains must segregate into chemically homogeneous regions with typical sizes of the order of the exciton diffusion length, in order to enhance the exciton dissociation probability thus avoiding wasteful radiative recombination events;

second, donor (acceptor) domains must be continuously connected to the anode (cathode) to favor efficient charge transport.[2,4] Figure 1 shows a schematic representation of a morphology that would satisfy these criteria: a lateral superlattice of donor−acceptor elongated domains with typical diameters of no more than 10−20 nm connected to the electrodes.[4c]

In this work we study by variable-temperature scanning tunneling microscopy (STM) the first stages in the growth of a self-assembled lateral superlattice of organic donor/acceptor areas, whose width is of about 10−20 nm, in good agreement with typical exciton diffusion lengths. Motivated by previous works, we attempted to use the nanometer-scale pattern provided by the well-known $22 \times \sqrt{3}$ "herringbone" reconstruction of the Au(111) surface as a template to steer the growth of the molecular species into one-dimensional (1D) molecular nanostructures with sizes in good registry with exciton diffusion lengths. Our experiments show that, although this simple picture is far from reality and the substrate cannot be regarded as an static checkerboard upon adsorption of the molecular species, molecule−molecule and molecule−substrate interactions conspire to steer a lateral segregation of the donor/acceptor blends into a long-range ordered superlattice of the kind described in Figure 1 as a highly desirable morphology for improving solar cell efficiencies. These results demonstrate that atomistic studies on the growth of organic thin films under ultrahigh vacuum (UHV) conditions can lead to the kind of accurate control

* Corresponding authors. E-mail: nazmar@quim.uacm.es. Address: Departamento de Química Orgánica, Facultad de Químicas, Universidad Complutense de Madrid, Avda. Complutense s/n, 28040 Madrid, Spain. Tel: +34 91 3944227. Fax: +34 91 3944103. E-mail: rodolfo.miranda@uam.es. Address: Departamento de Física de la Materia Condensada, Facultad de Ciencias, Universidad Autónoma de Madrid, Campus de Cantoblanco, 28049 Madrid, Spain. Tel: + 34 91 4974737. Fax: + 34 91 4973961.
† Departamento de Física de la Materia Condensada, Universidad Autónoma de Madrid, 28049 Madrid, Spain.
‡ Departamento de Química Orgánica, Universidad Complutense de Madrid.
§ Instituto de Ciencia de Materiales de Madrid−CSIC.
|| Instituto Madrileño de Estudios Avanzados en Nanociencia (IMDEA-Nanociencia), Madrid 28049, Spain.
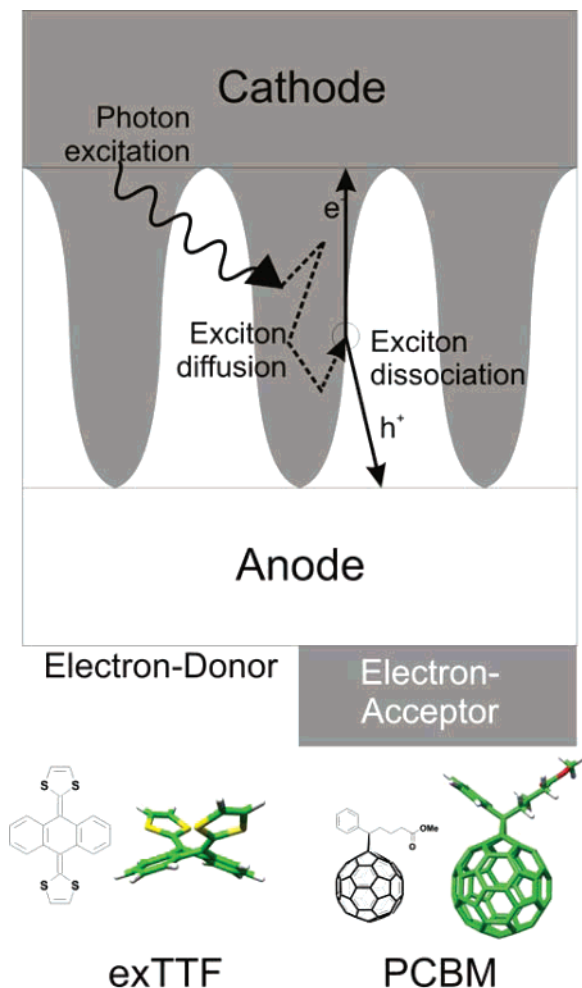
Figure 1. Schematic representation of the different steps in photoinduced charge separation in organic solar cells. Upon photon excitation, a tightly bound exciton is formed, that splits into free charge carriers after diffusing to a nearby donor/acceptor interface. Maximizing the solar cell efficiency requires, thus, to maximize the area of the donor/acceptor interface, to decrease the size of pure donor and pure acceptor areas down to dimensions of the order of the exciton diffusion length to avoid radiative recombination, and to preserve electrical connection between the interfaces and the electrodes. The chemical structures of the electron-donor (exTTF) and -acceptor (PCBM) molecules used in this study are included. For exTTF, carbon atoms are shown in green, hydrogen in white, and sulfur in yellow.

over the film morphology that is needed to improve the efficiency of electronic and optoelectronic organic devices.

The molecular species considered here are 2-[9-(1,3-dithiol-2-ylidene)anthracen-10(9H)-ylidene]-1,3-dithiole (exT-TF) (Figure 1) as the electron donor[5] and the fullerene derivative phenyl-C_{61}-butyric acid methyl ester (PCBM) (Figure 1) as the electron acceptor.[6] exTTF is a butterfly shaped electron-donor endowed with four sulfur atoms located on the two dithiole rings, which are expected to bind strongly to the Au(111) surface and with the two benzene rings forming a concave surface in an opposite orientation. PCBM is currently the most common organic acceptor used in photovoltaic applications.[1a,c,4b] The most important interaction expected between PCBM and exTTF is the $\pi-\pi$ interaction between the fullerene moiety and the benzene

rings of exTTF, as is the case for exTTF-based tweezers, capable of binding efficiently to C_{60} molecules.[7]

The chosen substrate, Au(111), reconstructs by increasing the atomic density at the surface with respect to a (111) plane in the bulk.[8] The reconstruction has a primary structure by which the surface topmost layer of atoms is uniaxially compressed by 4.5% with respect to the underlying bulk Au lattice. The change in the lattice parameter at the surface makes it impossible for the surface atoms to preserve the face-centered cubic (fcc) stacking characteristic of bulk Au, so that only a fraction of the atoms occupy fcc positions, another fraction occupies hexagonal close packed (hcp) sites, and fcc and hcp areas are separated by the so-called soliton walls (see Figure 2a). The reconstruction can appear in three orientational domains separated by the so-called elbows. Reconstructed, clean Au(111) shows a secondary "herringbone" structure in which the elbows are aligned along a line that forms 120° with the two soliton wall directions. It has been previously shown that the elbows act as nucleation centers, and the secondary structure of the herringbone templates the growth of ordered arrays of inorganic[9] and organic[10] nanostructures. The interisland distance reflects, thus, the interelbow distance, which is known to depend on preparation conditions and applied surface stress but generally is in the range of 10−20 nm. If the herringbone secondary structure templated the growth of the donor and acceptor molecules on Au(111) in the same manner, it would result in a lateral superlattice with sizes of the order of the exciton diffusion length.

Preparation of thin films and STM experiments were carried out in a UHV chamber with a base pressure of 2×10^{-10} Torr and equipped with standard facilities for metal surface preparation, two low-temperature effusion cells ($T < 800$ °C), and an Aarhus-type variable-temperature (down to 150 K), fast-scanning scanning tunneling microscope purchased from SPECS. Atomically clean, crystalline Au(111) surfaces were prepared by standard sputter/anneal procedures (sputter at 1 kV for 15 min followed by annealing to 800 K for another 15 min), which resulted in large terraces (about 200 nm wide), separated by monatomic steps and displaying the 22 × $\sqrt{3}$ herringbone reconstruction. exTTF and PCBM were deposited from two separate glass crucibles resistively heated at 400 and 500 K, respectively, onto the clean Au(111) substrate, that was held at room temperature. While exTTF could be imaged at room temperature, both PCBM and mixed films measurements were carried out at low temperature. Tunneling conditions are chosen so as to not disturb individual molecules ($V \approx 1$ V bias and $I \approx 100-500$ pA).

For the adsorption of PCBM molecules the templating role of reconstructed Au(111) works well. Both intermolecular and molecule−substrate interactions are weak, as evidenced by the fact that, for coverages below 1 ML, STM images measured at room temperature do not reveal any feature related to individual molecules or supramolecular aggregates other than an enhanced noise level typical of non-nucleated diffusing molecules;[11] the existence of adsorbed molecules is nevertheless confirmed by STM images recorded at lower
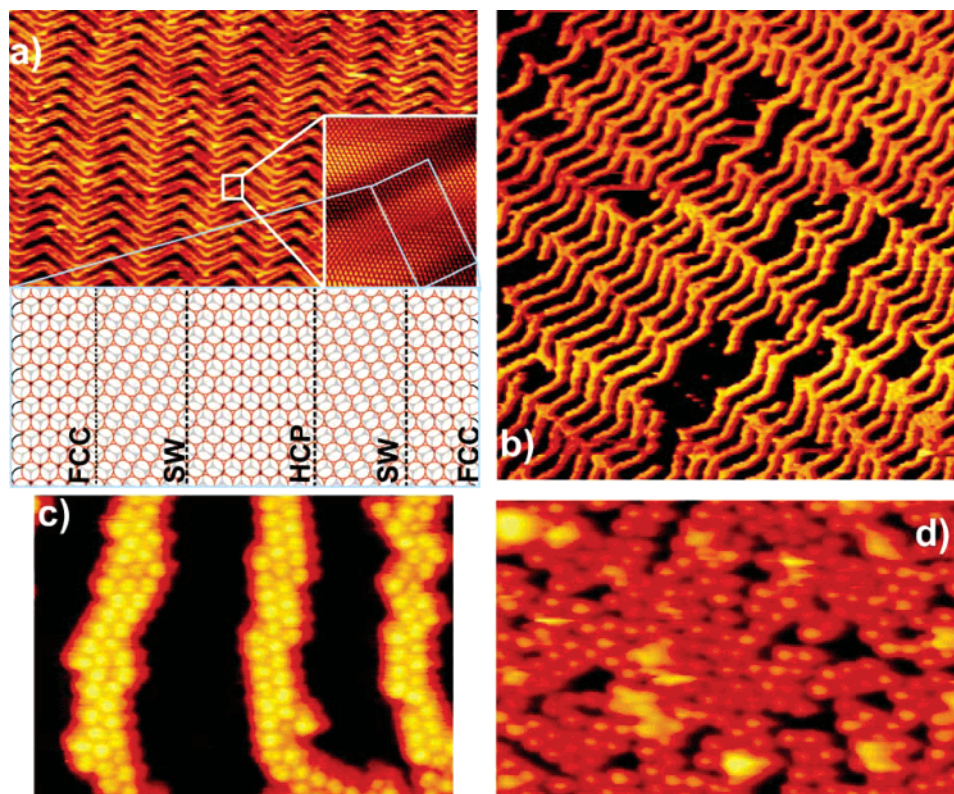
Figure 2. The "herringbone" reconstruction and its templating effect on the growth of PCBM. (a) STM image and schematic model of the herringbone reconstruction of the Au(111) surface (FCC and HCP stands for areas in which the atoms are stacked in fcc or hcp positions, respectively, while SW stands for soliton wall). The inset shows an atomically resolved image of the reconstruction. (b) 235×264 nm^2 STM image of the nanoscale "spider-web" obtained by decorating the FCC areas of the herringbone reconstruction with PCBM molecules. (c) High-resolution image of the PCBM molecular arrangement. (d) 59×42 nm^2 STM image of the high-coverage random-close packing phase of PCBM/Au(111). The samples imaged in (b), (c), and (d) were grown with the substrate kept at RT, but the STM images were taken 150 K.

temperatures (150 K) on the same sample (see parts b and c of Figure 2). Thus, PCBM molecules do not desorb at room temperature, but their interaction energy is so small compared to $k_{B}T$ that they behave as a highly mobile two-dimensional (2D) gas. Imaging at 300 K is only successful for coverages close to completion of a monolayer of PCBM molecules, when the surface mobility is sterically hindered. At 150 K, PCBM forms molecular double rows that adapt to the primary structure of the reconstruction by adsorbing only on the fcc areas of the intact herringbone structure. This is in sharp contrast with nonfunctionalized C$_{60}$, which self-assembles into close-packed hexagonal islands on Au(111) from very low coverages.[12] Thus, for coverages up to 0.4 ML, PCBM molecules decorate exclusively the fcc areas of the reconstruction, leading to the nanoscale "spider-web" structure depicted in parts b and c of Figure 2. At coverages higher than the available fcc sites, intermolecular interactions prevail and, close to 1 ML, a disordered structure is found, which only exhibits a short-range hexagonal order reminiscent of the hexagonal close-packing of C$_{60}$ on Au(111) (see Figure 2d).

The simple substrate-templated growth described for PCBM, however, cannot be extended to the adsorption of exTTF molecules on Au(111). Figure 3 shows the growth of exTTF on Au(111) at increasing coverages. For 0.3 ML, the surface morphology observed at room temperature

consists of exTTF stripe islands (darker areas of Figure 3a), separated by exTTF-free areas in which only bare gold and strike noise (as in the case of PCBM at room temperature) can be observed (see Figure 3a). exTTF islands can be easily recognized by STM due to their particular molecular organization, consisting of an ordered array of 1D molecular rows, and the peculiar appearance of individual molecules in high-resolution STM images (see the inset in Figure 3a). The molecular rows follow the compact[110] directions, and thus they form an angle of 30° with the domain-wall directions. The long edges of the exTTF islands run parallel to lines joining the elbows of the reconstruction. Interestingly, the lateral periodicity of the reconstruction's elbows is severely distorted underneath the exTTF-covered areas, in such a way that no elbow can be found underneath a single-domain exTTF island, as they are pushed away toward island edges or domain boundaries.

Thus, exTTF islands not only do not mirror the geometry of the surface's reconstruction but also they are able to modify it. The ability of exTTF to act on the reconstruction of Au(111) implies a significantly strong adsorbate−substrate interaction, which is further supported by the fact that exTTF molecules can be observed at room temperature by STM even at submonolayer coverage. The Au(111) unreconstructed surface is under substantial tensile stress, which is reduced upon reconstruction and increasing the atomic
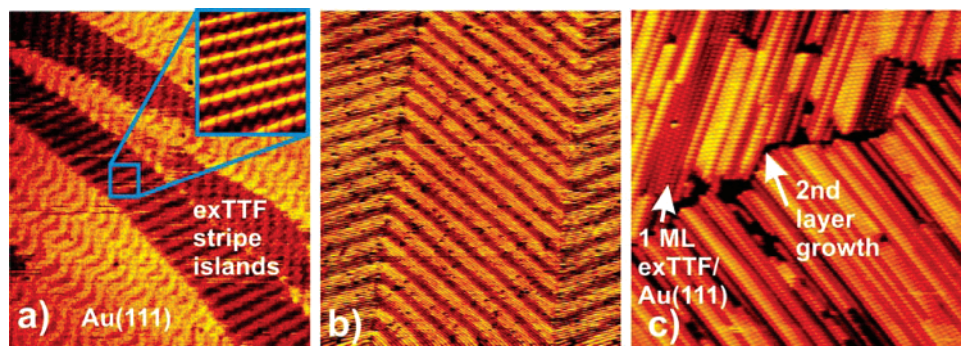
Figure 3. Growth morphology of exTTF thin films deposited on Au(111) at 300 K. (a) 176×198 nm^2 STM image of 0.3 ML. The exTTF areas are imaged darker and submolecular resolution is shown in the inset. The herringbone reconstruction can still be seen below the exTTF-covered areas, but the elbows are not present underneath the molecular islands. (b) 118×132 nm^2 STM image of 1 ML exTTF. The islands coalesce, and the elbows are restricted to the domain frontiers. (c) 59×66 nm^2 STM image for a coverage above 1 ML. Growth of second and third layers can be observed. The images were taken at room temperature. There is no change in the images upon lowering the temperature.

density at the surface.[13] The modification that the herringbone reconstruction undergoes upon exTTF adsorption is probably due to a further relaxation of the stress that removes partially the energetic need for the secondary structure of the reconstruction. The elbows of the Au(111) reconstruction have also been observed to disappear under uniaxial compression of the surface.[14] Notice that the modification of the secondary elbow structure of the herringbone reconstruction upon exTTF adsorption implies a breakdown of the surface templating assumption. Nevertheless there is still a very important influence of the reconstruction on the exTTF stripe-island morphology: instead of isotropic or hexagonal islands, as might be expected for a fcc(111) surface, it self-assembles into stripe islands in which the preferential growth direction is the one in which the elbows are aligned.

Upon completion of the first monolayer, the islands have coalesced, forming alternating stripes with different domain orientations and a typical width of 50 nm. The periodicity of the reconstruction's primary structure can still be observed as an extra corrugation superimposed to the molecular rows within each exTTF stripe domain (see Figure 3b). As was the case for submonolayer coverage, no elbow can be found in the interior of each stripe domain, as their existence is restricted to the boundaries between molecular domains. The growth of exTTF can be continued beyond 1 ML. Coverages up to 3 ML can be studied by STM by using suitably soft tunneling conditions ($It \approx 50$ pA, bias ≈ 1 V). Second layer islands grow in good registry with the first monolayer, and the islands are again elongated, aligned with the directions of the molecular rows of 1ML exTTF/Au(111) (Figure 3c). Molecules on the second and third monolayers also form well ordered 1D rows, but their lateral arrangement lacks the long-range order observed of the first monolayer (see Figure 3c). The ease with which second and even third layer exTTF molecules can be observed by STM implies a good electronic coupling and a strong bonding between consecutive layers

The influence of the herringbone reconstruction on the morphology of exTTF islands and the difference in bonding strength with Au(111) between PCBM and exTTF can still be used to steer the nanoscale morphology of exTTF/PCBM blends into a lateral superlattice like the one described in Figure 1. The stronger interaction of exTTF with Au implies a dominating role for this molecule to form the striped structures, leaving only the space between the exTTF stripes for the disordered PCBM close packing. As shown in Figure 4, this expectation is fulfilled by the experiments. Figure 4a shows the result of adding, at room temperature, about 0.6 ML of exTTF on top of the nanoscale spider-web PCBM structure depicted in Figure 2b (coverage of about 0.5 ML). Two distinct areas can be distinguished in the large-scale STM images: a well ordered area with a molecular structure identical to that shown by exTTF and where the elbow-free herringbone reconstruction underneath can be recognized as a long-period corrugation of the molecular rows, and a disordered area reminiscent of the high-coverage PCBM phase described in Figure 2d. The typical width of each area is about 20 nm. The ordered and disordered areas are assigned to pure exTTF molecules with a local thickness in excess of 1 ML and disordered PCBM molecules, respectively. Changing the order of the deposition, i.e., depositing about 0.5 ML exTTF first and then a submonolayer amount of PCBM, does not substantially alter this result (not shown).

This peculiar nanoscale phase segregation can be understood as follows. First, exTTF and PCBM do not show a tendency to mix, in good agreement with previous results observed in solution. Second, PCBM molecules are highly mobile at room temperature (RT), which is the temperature at which the PCBM/Au(111) substrate is held during deposition of exTTF. Since the stronger interaction of exTTF leads to self-assembled stripe islands that can be observed at RT, exTTF starts nucleating and forming the stripe islands, while PCBM molecules behave like a 2D gas on the Au-(111) surface. As exTTF coverage increases, the space left for the PCBM 2D molecular gas decreases until the concentration of PCBM molecules is so large that it cannot behave as a gas any longer, i.e., the density of PCBM molecules roughly equals the reciprocal of the molecular volume. The only area in which such a disordered PCBM 2D solid could stay is the area between adjacent exTTF stripe islands, which must then have a stripe morphology as well.
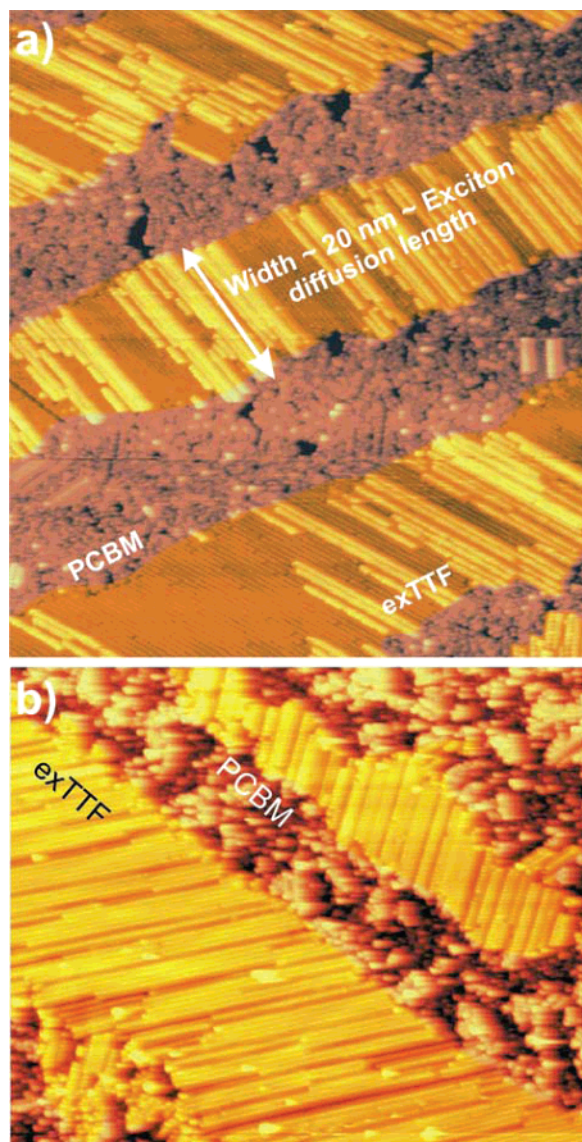
Figure 4. Lateral nanoscale organic donor/acceptor superlattice. (a) Nanoscale segregation of electron-donor/electron-acceptor molecules on Au(111) (118×132 nm^2). Since both PCBM and exTTF molecules are imaged with similar heights, a semitransparent color has been superimposed on the disordered PCBM areas to enhance visibility. The width of the exTTF stripes is about 20 nm, of the same order aas typical exciton diffusion lengths, and there exist a large acceptor/donor interface, as required for optimum solar-cell performance. (b) Further deposition of 0.5 ML exTTF on the sample described in (a) (118×115 nm^2). The selective adsorption of excess exTTF molecules on areas previously covered by exTTF molecules implies that this morphology can be extended beyond the first monolayer.

Thus the joint effect of molecule−substrate interactions (leading to striped morphology of exTTF islands and to a high mobility of PCBM molecules at RT) and molecule−molecule interactions (leading to PCBM/exTTF segregation, and strongly bound exTTF islands which are stable at room temperature) leads to the formation of the lateral superlattice shown in Figure 4.

The presence of second layer areas exclusively on the exTTF islands is a signal of the strong interaction among the exTTF molecules. As a consequence, the growth morphology and phase separation remain almost intact upon increasing the coverage. Figure 4b shows the result of depositing an additional 0.4 MLs of exTTF on the surface of Figure 4a. Although the width of the exTTF islands has increased slightly (which has made some of the PCBM molecules to jump to the second level), the most notorious change is their growth in height, now being almost completely two layers high with a significant portion of third layer. Although with STM alone it is impossible to ascertain how far the template effect of the substrate surface will dominate the mixed film structure, these results indicate that phase separation is an intrinsic property of the blend morphology.

As discussed above, the characteristic width of the exTTF and PCBM stripes is about 20 nm, which compares well with typical exciton diffusion lengths. Both exTTF and PCBM stripes extend laterally over micrometer distances and the morphology is statistically the same in all explored regions of the Au surface. These morphological features are ideal for the construction of highly efficient solar cells. Further experiments for the assessment of the optoelectronic behavior of the films grown by this method are underway. The applicability of the method to other metallic substrates with higher or lower work function needs to be verified. It will rely on the possibility of employing nanostructured or reconstructed surfaces provided with similar ordered dislocation patterns but widely different electronic structures at their surfaces,[15] such as Ag/Cu(111), Cu/Ru(0001), Pt/Cu(111), or Pt/Pt(111). We expect that similar and even more refined approaches will be exploited in the near future, further boosting the search for the optimum morphology of highly efficient organic solar cells.

References

(1) (a) Yu, G.; Gao, J.; Hummelen, J. C.; Wudl, F.; Heeger, A. J. *Science* **1995**, *270*, 1789−1791. (b) Halls, J. J. M.; Walsh, C. A.; Greenham, N. C.; Marseglia, E. A.; Friend, R. H.; Moratti, S. C.; Holmes, A. B. *Nature* **1995**, *376*, 498−500. (c) Brabec, C. J.; Sariciftci, N. S.; Hummelen, J. C. *Adv. Funct. Mater.* **2001**, *11*, 15−26.
(2) Nelson, J. *Curr. Opin. Solid State Mater. Sci.* **2002**, *6*, 87−95 (2002).
(3) Peumans, P.; Yakimov, A.; Forrest, S. R. *J. Appl. Phys.* **2003**, *93*, 3693−3723.
(4) (a) Yang, F.; Shtein, M.; Forrest, S. R. *Nat. Mater.* **2005**, *4*, 37−41. (b) Ma, W.; Yang, C.; Gong, X.; Lee, K.; Heeger, A. J. *Adv. Funct. Mater.* **2005**, *15*, 1617−1622. (c) Sylvester-Hvid, K. O.; Rettrup, S.; Ratner, M. A. *J. Phys. Chem. B* **2004**, *108*, 4296−4307.
(5) (a) Yamashita, Y.; Kobayashi, Y;, Miyashi, T. *Angew. Chem., Int. Ed. Engl.* **1989**, *28*, 1052−1053. (b) Martin, N.; Sánchez, L.; Seoane, C.; Ortí, E.; Viruela, P. M.; Viruela, R. *J. Org. Chem.* **1998**, *63*, 1268−1279.
(6) Hummelen, J. C.; Knight, B. W.; LePeq, F.; Wudl, F.; Yao, J.; Wilkins, C. L. *J. Org. Chem.* **1995**, *60*, 532−538.
(7) Perez, E. M.; Sanchez, L.; Fernandez, G.; Martin, N. *J. Am. Chem. Soc.* **2006**, *128*, 7172−7173.
(8) Barth, J. V.; Brune, H.; Ertl, G.; Behm, R. J. *Phys. Rev. B* **1990**, *42*, 9307−9318.

(9) Fruchart, O.; Klaua, M.; Barthel, J;, Kirschner, J. *Phys. Rev. Lett.* **1999**, *83*, 2769−2772.

(10) Clair, S.; Pons, S.; Brune, H.; Kern, K.; Barth, J. V. *Angew, Chem., Int. Ed.* **2005**, *44*, 7294−7297.

(11) Schunack, M.; Petersen, L.; Kühnle, A.; Lægsgaard, E.; Stensgaard, I.; Johannsen, I.; Besenbacher, F. *Phys. Rev. Lett.* **2001**, *86*, 456−459.

(12) Altman, E. I.; Colton, *Phys. Rev. B* **1993**, *48*, 18244−18249.

(13) Bach, C. E.; Giesen, M.; Ibach, H.; Einstein, T. L. *Phys. Rev. Lett.* **1997**, *78*, 4225−4228.

(14) Schaff, O.; Schmid, A. K.; Bartelt, N. C.; de la Figuera, J.; Hwang, R. Q. *Mat. Sci. Eng. A* **2001**, *319−321*, 914−918.

(15) Calleja, F.; García-Suárez, V. M.; Hinarejos, J. J.; Ferrer, J.; Vázquez, de Parga, A. L.; Miranda, R. *Phys. Rev. B* **2005**, *71*, 125412.

NL070897Z